

Giant planet formation in the solar system

A. Raorane^a, R. Brasser^{b,c}, S. Matsumura^d, T. C. H. Lau^e, M. H. Lee^f, A. Bouvier^g

^aDepartment of Earth and Climate Science, IISER Pune, Dr. Homi Bhabha Rd., Pune, 411008, India

^bHUN-REN Research Centre for Astronomy and Earth Sciences; MTA Centre of Excellence, 15-17 Konkoly Thege Miklos Rd., Budapest, 1121, Hungary

^cCentre for Planetary Habitability, University of Oslo, Sem Saelands vei 2A, Oslo, 0371, Norway

^dSchool of Science and Engineering, University of Dundee, Dundee, DD1 4HN, UK

^eUniversity Observatory, Faculty of Physics, Ludwig-Maximilians-University Munich, Scheinerstr. 1, Munich, 81679, Germany

^fDepartment of Earth Sciences and Department of Physics, The University of Hong Kong, Pokfulam Rd., Hong Kong, Hong Kong

^gBayerisches Geoinstitut, University of Bayreuth, Universitätsstrasse 30, Bayreuth, 95447, Germany

Abstract

The formation history of Jupiter has been of interest due to its ability to shape the solar system's history. Yet little attention has been paid to the formation and growth of Saturn and the other giant planets. Here we explore through N -body simulations the implications of the simplest disc and pebble accretion model with steady-state accretion on the formation of the giant planets in the solar system. We conducted a statistical survey of different disc parameters and initial conditions of the protoplanetary disc to establish which combination best reproduces the present outer solar system. We examined the effect of the initial planetesimal disc mass, the number of planetesimals and their size-frequency distribution slope, pebble accretion prescription and sticking efficiency on the likelihood of forming gas giants and their orbital distribution. The results reveal that the accretion sticking efficiency is the most sensitive parameter to control the final masses and number of giant planets. We have been unable to replicate the formation of all three types of giant planets in the solar system in a single simulation. The probability distribution of the final location of the giant planets is approximately constant in $\log r$, suggesting there is a slight preference for formation closer to the Sun but no preference for more massive planets to form closer. The eccentricity distribution has a higher mean for more massive planets indicating that systems with more massive planets are more violent. We compute the average formation time for proto-Jupiter to reach 10 Earth masses to be $\langle t_{c,J} \rangle = 1.1 \pm 0.3$ Myr and for proto-Saturn $\langle t_{c,S} \rangle = 3.3 \pm 0.4$ Myr, while for the ice giants this increases to $\langle t_{c,I} \rangle = 4.9 \pm 0.1$ Myr. The formation timescales of the cores of the gas giants are distinct at $> 95\%$ confidence, suggesting that they formed sequentially.

Keywords: Pebble accretion, Gas giant, numerical simulation, protoplanetary disc

1. Introduction

One of the remarkable features of the solar system is its diverse ensemble of planets. Particularly notable is the presence of giant planets of differing sizes and orbital distance. Planetary formation within protoplanetary discs is a complex process that unfolds across varying temporal and spatial scales (e.g. Morbidelli et al., 2012). An important step of this process is the growth of dust grains, which gradually coalesce into larger meter-sized boulders through successive collisions (e.g. Johansen et al., 2007).

Various mechanisms have been proposed to elucidate the subsequent formation of planetesimals. These mechanisms include gravitational collapse within exceptionally dense regions of the disc (Goldreich and Ward, 1973), the formation of compact clusters composed of aerodynamically sorted particles (Cuzzi et al., 2008), gravitational instability coupled with collisional accretion (Weidenschilling, 1980), and fragmentation processes within self-gravitating protoplanetary discs (Rice et al., 2006). Johansen et al. (2007) conducted simulations demonstrating the efficient gravitational collapse of boulders within locally overdense regions situated in the midplane of

the disc. This collapse is facilitated by transient high-pressure regions and streaming instability.

Once planetesimals are formed, they may merge to form larger bodies. The classical core accretion model presents the theory of giant planet formation that begins with planetesimal accretion (Pollack et al., 1996). However, it estimates that a 5-Earth mass (M_{\oplus}) planetary core would take up to 50 Myr to form at Jupiter's and Saturn's regions for typical solid surface densities (Pollack et al., 1996). These timescales are much longer than the inferred lifetime of nebular gas, which is between 0.1 Myr and 10 Myr, determined by observations of young stars similar to the Sun (Mamajek, 2009). Additionally, Levison et al. (2010) have shown that, in the outer solar system, core accretion simulations lead to the early planetesimal-driven migration of the growing cores, resulting in the formation of many hot super-Earths and gas giants. These studies suggest that the cores of gas giants, as in the solar system, cannot be formed by planetesimal accretion.

The Very Large Array Observations have shown large populations of grains with the sizes ranging from millimetres

to tens of centimetres in discs around other stars; these objects are referred to as ‘pebbles’ (e.g. Testi et al., 2003; Wilner et al., 2005). Micron-sized dust grains can grow into pebbles via coagulation until effectively limited by radial drift (Mumma et al., 1993; Weidenschilling, 1977). Accretion of these pebbles (Ormel and Klahr, 2010; Lambrechts and Johansen, 2012) by planetesimals has progressively gained acknowledgment as a viable model for the formation of gas giant planets due its efficiency in forming planetary cores. Johansen and Lacerda (2010) conducted hydrodynamical simulations to investigate the process of pebble and rock accretion onto nascent protoplanets in gaseous discs. Meanwhile, Ormel and Klahr (2010) demonstrated the high efficiency of pebble accretion, primarily attributed to the increased cross-section in the settling regime. The term ‘pebble accretion’ was coined by Lambrechts and Johansen (2012) to characterize the process wherein small pebbles are amassed by existing planetesimals, implying that this rapid accretion might facilitate the formation of giant planet cores.

Several studies have conducted numerical simulations to explore pebble accretion models for giant planet formation employing simple disc models. Levison et al. (2015) studied the formation of gas giants where pebbles are formed over the lifetime of the disc, and showed the formation of gas giants between 5 and 15 astronomical units (au) from the Sun within 10 Myr. Matsumura et al. (2017) adapted the Symplectic Massive Body Algorithm (SyMBA) (Duncan et al., 1998) to incorporate key planet formation processes, including pebble accretion, planet migration, and gas accretion. However, they did not form any gas giants at the end of the 50-Myr simulations due to the rapid migration of planetary cores to the inner edge of the disc, in contrast to Levison et al. (2015) where migration is not considered. Matsumura et al. (2021) built on the results of Matsumura et al. (2017) and were successful in reproducing orbital distribution trends of extra-solar gas giants. When the same model was applied to the solar system, rapid migration of giant planet cores into inner solar system was seen (Lau et al., 2024).

In this work, the implications of the simplest disc and pebble accretion model are being investigated in more detail, with steady-state accretion onto the star and an assumed ringed structure in the disc at 5 au (Brasser and Mojzsis, 2020). No additional ringed features are assumed to exist, because the effect of a ringed structure in the disc on pebble accretion is not yet well understood. It is further assumed that no additional material is added to the disc from the interstellar medium as it evolves. From this setup we predominantly form planets whose mass is in between that of Saturn and Jupiter.

The paper is structured in the following manner. In Section 2, we describe the model used, followed by the numerical methods and initial conditions for the simulations in Section 3. In Section 4, we illustrate the orbital distribution of the giant planets formed within our systems. Additionally, we depict the impact of varying parameter values related to the planetesimal disc and

accretion efficiencies on planet formation probabilities. Finally, we present the timelines for core formation in the cases of Saturn and Jupiter, as well as the duration for the cores to accumulate a gas envelope. We discuss the results further in Section 5, and summarise our findings in Section 6.

2. Theory

In this work, we used the same disc model as in Matsumura et al. (2021), which is adopted from Ida et al. (2016) as summarized below.

2.1. Gas disc

The disc evolution is described by the diffusion equation (Lynden-Bell and Pringle, 1974) for the disc’s surface mass density Σ_g

$$\frac{\partial \Sigma_g}{\partial t} = -\frac{1}{r} \frac{\partial}{\partial r} \left[3r^{1/2} \frac{\partial}{\partial r} (\Sigma_g \nu r^{1/2}) \right] \quad (1)$$

where ν is the disc’s viscosity representing the accretion rate. The gas accretion rate onto the star (Shakura and Sunyaev, 1973), \dot{M}_* is related to the gas surface density, Σ , and scale height of the disc, H , via

$$\dot{M}_* = 3\pi\alpha_{\text{acc}}\Sigma H^2\Omega_K, \quad (2)$$

where $\Omega_K = \sqrt{GM_*/r^3}$ is the Kepler frequency. Classically, the parameter α_{acc} is a measure for the global angular momentum transfer of the disc, which is parameterized by (Shakura and Sunyaev, 1973)

$$\nu = \alpha_{\text{acc}}c_s^2\Omega_K^{-1}. \quad (3)$$

Following Ida et al. (2018) and Bitsch et al. (2019), the work by Matsumura et al. (2021) adopted a two- α disk model which mimics the wind-driven accretion disc with a low-level of turbulence. As pointed out by Matsumura et al. (2021), α_{acc} is due to the effect that is driving the accretion (be it either magnetic disc winds, viscosity, or something else). In contrast, the effect of disc turbulence is represented by α_{turb} , which is generally a small parameter since disc turbulence is expected to be weak (Bai, 2017).

The disc scale height $H = c_s/\Omega_K$, where $c_s = \sqrt{\gamma k_B T/2.3m_p}$ is the sound speed, $k_B = 1.381 \times 10^{-23} \text{ m}^2 \text{ kg s}^{-1} \text{ K}^{-2}$ is the Boltzmann constant, m_p is the proton mass, the mean atomic mass of the gas is assumed to be 2.3 and $\gamma = 7/5$ is the ratio of specific heats of the gas molecules. The stellar accretion rate in the self-similar solution decreases with time as (Hartmann et al., 1998)

$$\dot{M}_* = \frac{M_d}{(2q+1)t_{\text{diff}}} \left(\frac{t}{t_{\text{diff}}} + 1 \right)^{-(2q+2)/(2q+1)} \quad (4)$$

where M_d is the mass of the disc, t_{diff} is the diffusion time, and $q = -d \ln T/d \ln r$ is the negative temperature gradient. In the irradiative regime of the disc in the giant planet region $q = 3/7$ (Ida et al., 2016) (see below) and

$(2q + 2)/(2q + 1) = 20/13 \approx 1.53$. Most observed discs have a mass that's about 3%-8% of the stellar mass (Manara et al., 2016). For a disc mass of $M_d = 0.05 M_\odot$ we have initially $\dot{M}_* = 5.3 \times 10^{-8} M_\odot \text{ yr}^{-1}$ if $t_{\text{diff}} = 0.5 \text{ Myr}$ and the accretion rate onto the star becomes approximately $2.5 \times 10^{-9} M_\odot \text{ yr}^{-1}$ after about 5 Myr of evolution, a little later than the inferred disappearance of the disc from meteorite magnetic fields (Wang et al., 2017).

In the giant planet region, the disc mid-plane temperature can be approximated by (Ida et al., 2016)

$$T = 150 \left(\frac{L_*}{L_\odot} \right)^{2/7} \left(\frac{M_*}{M_\odot} \right)^{-1/7} \left(\frac{r}{1 \text{ au}} \right)^{-3/7} \text{ K}, \quad (5)$$

where r is the distance to the Sun. To simplify the formulae, we define

$$\alpha_3 \equiv \frac{\alpha_{\text{acc}}}{10^{-3}}, \quad (6)$$

$$\dot{M}_{*8} \equiv \frac{\dot{M}_*}{10^{-8} M_\odot \text{ yr}^{-1}}. \quad (7)$$

With this temperature profile, one may compute the reduced scale height $h = H/r$ as

$$h = 0.029 \left(\frac{L_*}{L_\odot} \right)^{1/7} \left(\frac{M_*}{M_\odot} \right)^{-4/7} \left(\frac{r}{1 \text{ au}} \right)^{2/7}. \quad (8)$$

The gas surface density profile is

$$\Sigma = 1785 \left(\frac{L_*}{L_\odot} \right)^{-2/7} \left(\frac{M_*}{M_\odot} \right)^{9/14} \alpha_3^{-1} \dot{M}_{*8} \left(\frac{r}{1 \text{ au}} \right)^{-15/14} \text{ g cm}^{-2}. \quad (9)$$

2.2. Planet migration

In the simulations, the equation of motion incorporates planet-disc interactions based on gas disc torques and dynamical friction. We follow the prescription of Ida et al. (2020). The acceleration due to the gas is given by

$$\frac{d\vec{v}}{dt} = -\frac{v_k}{2\tau_a} \vec{e}_\theta - \frac{v_r}{\tau_e} \vec{e}_r - \frac{v_\theta - v_k}{\tau_e} \vec{e}_\theta - \frac{v_z}{\tau_i} \vec{e}_z \quad (10)$$

where, \vec{v} is the planetary velocity evaluated at the instantaneous orbital radius r , with v_r , v_θ , and v_z being its polar coordinate components defined with the unit vectors \vec{e}_r , \vec{e}_θ , and \vec{e}_z , respectively. Lastly, v_k is the Keplerian orbital speed evaluated at the instantaneous orbital radius r .

The evolution timescales for the semi-major axis, eccentricity, and inclination are expressed as follows:

$$\begin{aligned} \tau_a &= -(1 + 0.04K) \frac{t_{\text{wave}}}{2h^2} \\ &\times \left[\frac{\Gamma_L}{\Gamma_0} \left(1 - \frac{1}{C_M} \frac{\Gamma_L}{\Gamma_0} \sqrt{\hat{e}^2 + \hat{i}^2} \right)^{-1} + \frac{\Gamma_C}{\Gamma_0} \exp \left(-\frac{\sqrt{\hat{e}^2 + \hat{i}^2}}{e_f} \right) \right] \\ \tau_e &= 1.282(1 + 0.04K)t_{\text{wave}} \left[1 + \frac{1}{15}(\hat{e}^2 + \hat{i}^2)^{3/2} \right], \end{aligned} \quad (12)$$

$$\tau_i = 1.838(1 + 0.04K)t_{\text{wave}} \left[1 + \frac{2}{43}(\hat{e}^2 + \hat{i}^2)^{3/2} \right], \quad (13)$$

where eccentricities and inclinations scaled with h are defined as $\hat{e} = e/h$ and $\hat{i} = i/h$, respectively, and $e_f = 0.01 + h/2$ (Fendyke and Nelson, 2014) and $C_M = 6(2p - q + 2) = 156/7 \approx 22.3$ (Ida et al., 2020), where we assumed a steady state accretion disc so that the surface density slope $p = -d \ln \Sigma / d \ln r = 3/2 - q = 15/14$. The quantity Γ/Γ_0 represents a normalized torque, and the subscripts L and C, respectively, correspond to Lindblad and corotation torque. These were computed using the prescription of Paardekooper et al. (2011), in which the corotation torque also depends on the amount of saturation of the barotropic and entropic parts. The part of the torques dependent on temperature and surface density slopes q and p are $\Gamma_L/\Gamma_0 = 2.50 - 0.1p + 1.7q \approx 1.81$ and $\Gamma_C/\Gamma_0 = 2.73 + 1.08p + 0.87q \approx 1.95$ (Ida et al., 2020). Lastly, t_{wave} is the characteristic time of wave induction in the disc, which propels the migration, and is given in Tanaka et al. (2002) as

$$t_{\text{wave}} = \left(\frac{M_*}{m_p} \right) \left(\frac{M_*}{\Sigma a^2} \right) h^4 \Omega_K^{-1} \quad (14)$$

where m_p is the planetesimal or planet mass and M_* is the mass of the star/Sun. The factor K is related to gap opening and is given by (Kanagawa et al., 2018)

$$K = \left(\frac{m_p}{M_*} \right)^2 h^{-5} \alpha_{\text{turb}}^{-1}, \quad (15)$$

where α_{turb} represents the strength of the local disc turbulence, which we set to $\alpha_{\text{turb}} = 10^{-4}$. Gap opening becomes important when $K = 25$ which occurs when

$$m_p \sim 2.6 \left(\frac{\alpha_{\text{turb}}}{10^{-4}} \right)^{1/2} \left(\frac{h}{0.03} \right)^{5/2} \left(\frac{r}{1 \text{ au}} \right)^{5/8} M_\oplus. \quad (16)$$

The accretion parameter α_{acc} is computed from the disc model rather than treated as an input parameter (Matsumura et al., 2021).

2.3. Pebble accretion

Ida et al. (2019) and Matsumura et al. (2021) proposed a pebble accretion model that accounts for planet-disc interactions and the two- α model. The incorporation of these factors has led to efficient accretion, thereby enabling the formation of gas giant cores through pebble accretion within a time frame of 5 Myr.

(11) The pebbles are thought to form in a front that sweeps outwards (Lambrechts and Johansen, 2014). The pebble mass flux describes the pebble mass swept up by the pebble formation front per unit time as it sweeps through the disc (Lambrechts et al., 2014),

$$\dot{M}_F = 2\pi r_{\text{pff}} \Sigma_p \frac{dr_{\text{pff}}}{dt} \quad (17)$$

where Σ_p is the pebble surface density in the pebble migrating region. The pebble formation time, t_{pff} , and r_{pff} , the radius of the pebble formation front, are computed as (Ida et al., 2016)

$$r_{\text{pff}} = 100 f^{2/3} \left(\frac{t}{0.2 \text{ Myr}} \right)^{2/3} \left(\frac{Z_0}{10^{-2}} \right)^{2/3} \left(\frac{M_*}{M_\odot} \right)^{1/3} \text{ au} \quad (18)$$

$$t_{\text{pff}} = 2 f^{-1} \times 10^5 \left(\frac{Z_0}{10^{-2}} \right)^{-1} \left(\frac{r_{d,0}}{100 \text{ au}} \right)^{3/2} \left(\frac{M_*}{M_\odot} \right)^{-1/2} \text{ yr} \quad (19)$$

where Z_0 is the initial solid-to-gas ratio in the disc and is typically assumed to be 0.01. For high enough speed collisions, grains rebound or fragment rather than coagulate, which is called the bouncing or fragmentation barrier (Blum and Wurm, 2000). We model this inefficient coagulation through the sticking efficiency f of dust to pebbles, which is another input parameter.

To compute the flux of pebbles in the disc, we used the derivation by Matsumura et al. (2021), which yields

$$\begin{aligned} \dot{M}_F &= 0.021 f^{2/3} \left[\frac{\ln(R_{\text{peb}}/R_0)}{\ln 10^4} \right]^{-1} \left(\frac{T_2}{150 \text{ K}} \right)^{-1} L_{*0}^{-2/7} M_{*0}^{8/7} \\ &\times \alpha_3^{-1} \dot{M}_{*8} \left(\frac{Z_0}{0.01} \right)^2 \left(\frac{r_D}{1 \text{ au}} \right)^{-4/7} \\ &\times \left(\frac{t}{t_{\text{pff}}} \right)^{-8/21} M_\oplus \text{ yr}^{-1}, \end{aligned} \quad (20)$$

where $T_2 = 150 \text{ K}$ is the characteristic disc temperature due to stellar radiation, and R_0 and R_{peb} are the initial radii of dust particles and the pebbles when they start to migrate, respectively (Matsumura et al., 2021).

The rate of accretion from pebbles onto a planetesimal-sized or larger body is derived to be (Ida et al., 2016)

$$\dot{M}_{\text{core}} = \varepsilon \dot{M}_F, \quad (21)$$

where \dot{M}_F is the pebble mass flux. The accretion efficiency ε is given by (Ida et al., 2016)

$$\varepsilon = \min \left[1, \frac{C \hat{b}^2 \sqrt{1 + 4S^2}}{4 \sqrt{2\pi} S \hat{h}_p} \left(1 + \frac{3\hat{b}}{2\chi\eta} \right) \right], \quad (22)$$

where \dot{M}_F is the flux of pebbles through the disc; its temporal evolution depends on the gas accretion rate onto the star and the formation efficiency of pebbles. The other quantities in equation (22) are given by

$$\begin{aligned} b &= 2\kappa r_H S^{1/3} \min \left(\sqrt{\frac{3r_H}{\chi\eta r}} S^{1/6}, 1 \right), \\ \chi &= \frac{\sqrt{1 + 4S^2}}{1 + S^2}, \\ h_p &= \left(1 + \frac{S}{\alpha_{\text{turb}}} \right)^{-1/2} h \\ C &= \min \left(\sqrt{\frac{8}{\pi}} \frac{h_p}{b}, 1 \right), \\ \eta &= \frac{1}{2} h^2 \left| \frac{d \ln P}{d \ln r} \right| = \frac{39}{28} h^2 \end{aligned}$$

$$\ln \kappa = - \left(\frac{S}{S^*} \right)^{0.65},$$

$$S^* = \min(2, 4\eta^{-3}\mu),$$

where $\mu = m_p/M_*$, α_{turb} is the disc's turbulent viscosity, $r_H = r(\mu/3)^{1/3}$ is the Hill radius, P is the gas pressure and S is the Stokes number. Quantities with a circumflex are scaled by the distance to the star, and h_p is the scale height of the pebbles as they drift sun-ward through the disc.

An alternative prescription for the pebble accretion efficiency is given by Ormel and Liu (2018), who included combined effects of the planet's gravitational attraction and gas drag. They studied the 3D pebble accretion efficiency by considering the effects of eccentricity, inclination, and disc turbulence. When the planetesimal radius is small compared to the scale height of the pebble stream, the accretion is 3D and the efficiency in the settling regime is given by

$$\varepsilon = \frac{A_3}{\eta h_{p,\text{eff}}} \left(\frac{m_p}{M_*} \right) f_{\text{set}}^2 \quad (23)$$

where $A_3 = 0.39$ is a constant, $h_{p,\text{eff}}$ is the effective reduced pebble scale height, which accounts for the reduced interaction between pebble and planetesimal by either turbulent stirring of pebbles or planetesimal inclination, and $f_{\text{set}} = \exp[-0.5(\Delta v/v_*)^2]$ is the settling fraction. We further have $\Delta v = \max(0.76e, \eta)v_K$, which is the approach speed between the pebble and the planetesimal, and the settling velocity $v_* = (m_p/M_*)^{1/3} S^{-1/3} v_K$, where $v_K = r\Omega_K$ is the Kepler velocity. When $\Delta v \gg v_*$, the accretion is in the ballistic regime, and is highly inefficient. Furthermore $h_{p,\text{eff}} \approx h_p$ when $i_p \ll h_p$, and $h_{p,\text{eff}} \approx 1.25i_p$ when $i_p \gg h_p$. When the planetesimal mass grows large enough such that its diameter becomes comparable to the pebble scale height, the accretion is 2D and the efficiency becomes

$$\varepsilon = \frac{A_2}{\eta} \left[\frac{m_p}{M_*} \frac{\Delta v}{v_*} S^{-1} \right]^{1/2} f_{\text{set}}, \quad (24)$$

where $A_2 = 0.32$. The crossover between the two regimes in the low-eccentricity regime occurs when the mass of the planetesimal satisfies $m_p/M_* = \eta^3 S$. The quantity f_{set} is a complicated function of the planetesimal inclination and eccentricity, and the disc's turbulence, and we refer to Ormel and Liu (2018) for more details. We have implemented their full prescription in the software used in this work.

Pebble accretion occurs until the planet reaches the so-called pebble isolation mass (Lambrechts et al., 2014), after which it ceases due to turbulent wakes created in the disc by the planet. We are using the pebble isolation mass prescription of Ataiee et al. (2018), which yields

$$\frac{m_{\text{iso}}}{M_*} = h^3 \sqrt{0.01 + 37.3\alpha_{\text{turb}}} \left[1 + 0.2 \left(\frac{\sqrt{\alpha_{\text{turb}}(4 + S^{-2})}}{h} \right)^{0.7} \right], \quad (25)$$

which results in $\sim 10 - 20 M_\oplus$ in the region between 5 au and 25 au for the disc parameters we have chosen.

2.4. Gas envelope accretion

The nucleated instability model proposes that the formation of giant planets may occur when a solid protoplanet, commonly referred to as a core, reaches a critical mass and triggers rapid accretion of nebular gas, resulting in the formation of a massive gaseous envelope (Ikoma et al., 2000). The gas envelope accretion proceeds as

$$\frac{dM_{\text{env}}}{dt} \sim \frac{M_{\text{core}}}{\tau_g}. \quad (26)$$

The growth time of the gaseous envelope mass, τ_g , depends strongly on the core mass of the planet, moderately on the grain opacity, and weakly on the past core accretion process.

$$\tau_g = b \left(\frac{M_{\oplus}}{M_{\text{core}}} \right)^c \left(\frac{\kappa_{\text{gr}}}{1 \text{ cm}^2 \text{ g}^{-1}} \right) \text{yr} \quad (27)$$

where M_{core} is the core mass and κ_{gr} is the grain opacity. Typically $\log b = 8 - 10$ and $c = 2 - 4$ (Ikoma et al., 2000); for this study we set $\log b = 8$ and $c = 3$. The opacity was set to $1 \text{ cm}^2 \text{ g}^{-1}$; its value does not really matter due to the uncertainties in the values of b and c . Gas envelope accretion is restricted by gas flow to the star and gap opening in the disc by the growing planet. Combining these factors, gas accretion proceeds as (Ida et al., 2018)

$$\frac{dM_{\text{env}}}{dt} = \min \left[\frac{M_{\text{core}}}{\tau_g}, \dot{M}_*, f_{\text{gap}} \dot{M}_* \right], \quad (28)$$

where f_{gap} is a reduction factor due to gap opening of the growing planet (Ida et al., 2018), and is given by

$$f_{\text{gap}} = \frac{0.031}{(1 + 0.04K)h^4 \alpha_{\text{acc}}} \left(\frac{m_p}{M_*} \right)^{4/3}. \quad (29)$$

2.5. Parameter choice

The input disc mass and diffusion time are taken from observed disc masses and meteorite magnetic measurements that infer a dissipation time of the solar system's protoplanetary disc by about 4 Myr (Wang et al., 2017). The gas accretion parameters have a range of values in the literature. (e.g. Manara et al., 2016). The initial mass in planetesimals was somewhat arbitrarily chosen, but we wanted to ensure that we had a thousand to a few thousand planetesimals, and that there were large enough bodies that would grow fast enough to form gas giants before the end of the simulations. We were inspired by the initial conditions of Levison et al. (2015) regarding the initial planetesimal mass. Planetesimal formation simulations imply a somewhat shallow size-frequency distribution slope of -1.8 (Johansen et al., 2015), shallower than what we have used here; instead, our choice was informed by Levison et al. (2015) and the size-frequency distribution due to collisional grinding (Dohnanyi, 1969). We also noted during the test simulations that we produced no gas giants when the sticking efficiency was lower than 0.5.

3. Methods and initial conditions

To study the formation of giant planets and their evolution, we ran N-body simulations with SyMBAp, the parallel version of the software package SyMBA (Duncan et al., 1998; Lau and Lee, 2023). This code has been modified to include the forces from the gas disc, mass growth due to pebble accretion, and gas envelope accretion.

The parameter space required to generate the desired gas disc and initial conditions is extensive. The number of parameters utilized in this study is contingent upon the specific goals of the simulations. In Table 1 we list the free parameters in the problem. We chose to keep the quantities in the top five rows fixed because they are somewhat constrained by observations. The quantities in the bottom five rows are less well constrained, and therefore have been tested here, and their range of values that we have employed. The choices for disc mass, gas diffusion time and gas inner and outer edge were obtained from observational constraints (e.g. Manara et al., 2016), and from low- N simulations starting with 2-25 Ceres-mass planetary embryos, and tabulating which combinations yielded gas giant planets.

Following Levison et al. (2015) we began the simulations with an initial planetesimal disc. The assumption of a planetesimal disc is a key component of the model but not universally accepted: the spatial distribution (e.g. Drazkowska et al., 2016; Carrera et al., 2017; Schoonenberg et al., 2018; Lenz et al., 2019, 2020) and the condition for the formation of planetesimals through the gravitational collapse caused by the streaming instability (e.g. Carrera et al., 2015; Yang et al., 2017; Li and Youdin, 2021; Gerbig and Li, 2023) remain active topics of research.

We ran 840 simulations with 56 different parameter combinations, with most simulations initially having 1000 to 1200 self-gravitating planetesimals. In each simulation, the central object was a Sun-like star and the gas disc's inner boundary was fixed at 5 au, to comport with a hypothesised pressure maximum there (Brasser and Mojzsis, 2020) and to prevent giant planets migrating into the inner solar system. The orbital elements (semi-major axis, eccentricity, inclination, the longitude of the node, the argument of perihelion, and mean anomaly) are uniformly generated with their appropriate multiplicative factors and limits. The initial semi-major axes of the planetesimals ranged from 5 to 25 au. Every planetesimal was randomly assigned an initial eccentricity within the range of $e = [0, 0.001]$, an associated inclination of $i = 0.5e$ radians, and randomized phase angles.

The mass-radius relationship for planetesimals and planet cores that we use here is given by Seager et al. (2007). The following equation is satisfied by cold terrestrial planets $m_p < 20 M_{\oplus}$ of all compositions.

$$\log \left(\frac{R_p}{3.3 R_{\oplus}} \right) = k_1 + \frac{1}{3} \log \left(\frac{m_p}{5.5 M_{\oplus}} \right) - k_2 \left(\frac{m_p}{5.5 M_{\oplus}} \right)^{k_3} \quad (30)$$

Table 1: List of parameters and their range of values

No.	Parameter	Symbol	Unit	Literature Range	Used value(s)
1	Initial mass of gas disc	$M_{\text{disc},0}$	M_{\odot}	0.01 – 0.1	0.05
2	Gas disc diffusion timescale	t_{diff}	yr	10^{5-7}	5×10^5
3	Disc inner and outer edge	$r_{\text{in}}, r_{\text{out}}$	au	0.01 – 5, 100 – 500	5, 100
4	Disc turbulence parameter	α_{turb}	-	$10^{-(3-5)}$	10^{-4}
5	Gas accretion coefficients	b, c	-, -	$10^{8-10}, 2 - 4$	$10^8, 3$
6	Pebble accretion efficiency prescription	peb_flg	-	-	Ida (0), Ormel (1)
7	Sticking efficiency	f	-	0.5 – 1	0.5, 0.75, 1
8	Initial mass in planetesimals	m_{tot}	M_{\oplus}	0.01 – 4	0.5, 1, 4
9	Slope of planetesimal size distribution	β	-	2.5 – 4.5	2.5, 4.5
10	Initial number of planetesimals	N	10^3	-	1 – 1.2, 1.5, 2.4, 3.2, 4.5

where m_p and R are the mass and radius of the planet, and where $k_1 = -0.2095$, $k_2 = 0.0804$, and $k_3 = -0.3940$. For planets more massive than $5 M_{\oplus}$ we used the prescription $R = 1.65(m_p/5 M_{\oplus})^{1/2} R_{\oplus}$ (Weiss and Marcy, 2014).

The maximum mass of a planetesimal in the initial distribution is estimated by the equation (Matsumura et al., 2021)

$$M_{\text{plms,init}} \approx 13.8 \left(1 + \frac{\mathcal{S}}{\alpha_{\text{turb}}}\right)^{-3/2} L_{*0}^{3/7} M_{*0}^{-5/7} \left(\frac{r}{1 \text{ au}}\right)^{6/7} M_{\oplus}. \quad (31)$$

For reasonable values of $\mathcal{S} \sim 0.1-1$, $\alpha_{\text{turb}} = 10^{-4}$, $r = 10$ au and a bulk density of about 1500 kg m^{-3} , the maximum radius of planetesimals is about 2000 km. Our maximum adopted input value is usually 1500 km or 2500 km depending on initial disc mass and size-frequency distribution slope. We placed one planetesimal with a lunar mass and a radius of 2000 km near 5 au with the intention that this could become our Jupiter analogue (Brasser and Mojzsis, 2020).

The slope of the initial size-frequency distribution of the planetesimals is another free parameter. Both a shallow and a steep size distribution were tested. The total mass of the planetesimal disc, and the minimum and maximum radii of the planetesimals were kept as additional input parameters. The radii are generated from a truncated Pareto distribution using a random number as

$$r_p = r_{\text{min}} \zeta^{-1/\beta}, \quad (32)$$

where ζ is a random number from an uniform distribution between (0, 1) and β is the size-frequency distribution slope; if $r_p > r_{\text{max}}$ the procedure is restarted.

Simulations were run for 5 Myr with a time step of 0.1 yr. All bodies are self-gravitating. Bodies were removed when they were closer than 1 au or farther than 100 au from the Sun,

or underwent a collision.

The speed of SyMBAp, using 8 CPU cores on AMD EPYC 7H12 CPUs running at 3 GHz, in both gravity only mode and in pebble accretion with planet migration mode, is shown in Fig. 2, which depicts the number of steps per particle per second vs the number of bodies. The computational overhead due to pebble accretion and planet migration amounts to about 50% for $N \leq 512$. For this low number of planetesimals the number of steps per second decreases approximately as N^{-1} while for $N \geq 1024$ it decreases as the expected N^{-2} . Due to this rapid decline in speed, for most sets of the simulations, we kept the number of planetesimals between 1000 and 1500, but we have also run some sets with 2400, 3200 and 4500 planetesimals.

We used 8 cores per simulation. The simulation duration was typically 2 days for 1000 planetesimals and increased as N^2 , with high- N runs lasting up to 40 days. The parameter combinations used and analyzed in these simulations are presented in the figure (Figure 1). Fifty-six combinations of the following parameters were analysed: (a) sticking efficiency (f), (b) pebble accretion prescription peb_flg, (c) total initial planetesimal mass in disc (m_{tot}), (d) planetesimal size-frequency slope (β) and (e) initial number of planetesimals (N).

4. Results

In this section we present the outcomes of our numerical simulations. Before we get to that, we report on a phenomenon in the simulations that skewed the outcome due to our truncation of the gas disc at 5 au.

4.1. Truncated gas accretion

We truncated the gas disc in our simulations at 5 au to mimic the pressure maximum postulated by Brasser and Mojzsis

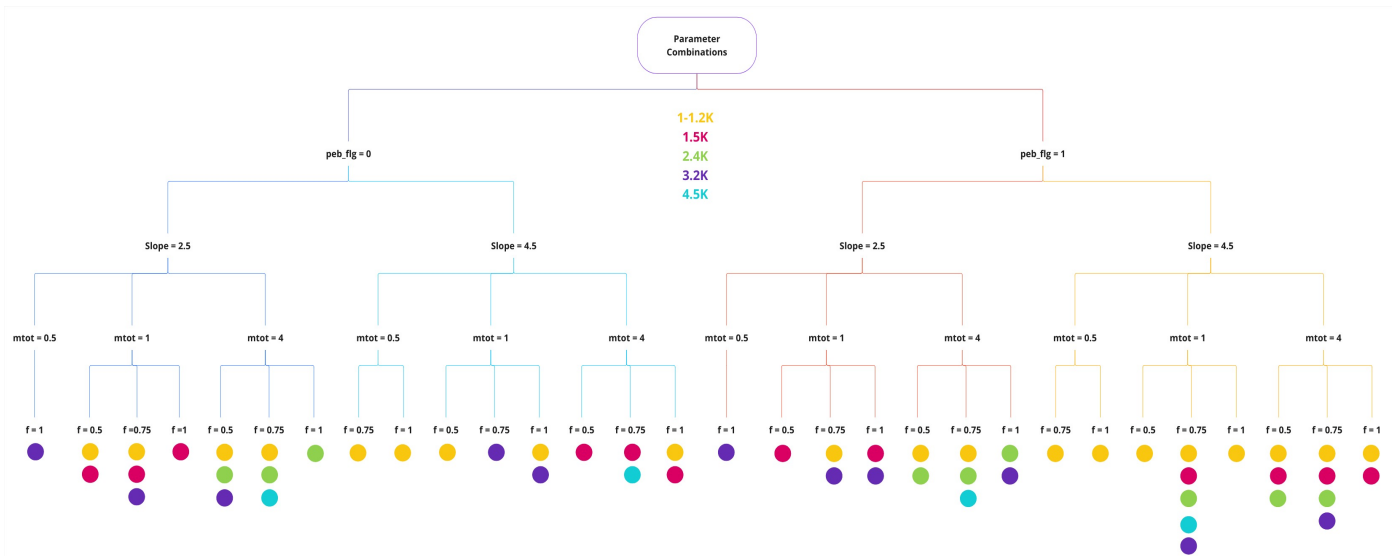


Figure 1: Parameter Combination for Production Simulations. Circles represent a set of 15 runs. The colours correspond to the number of planetesimals.

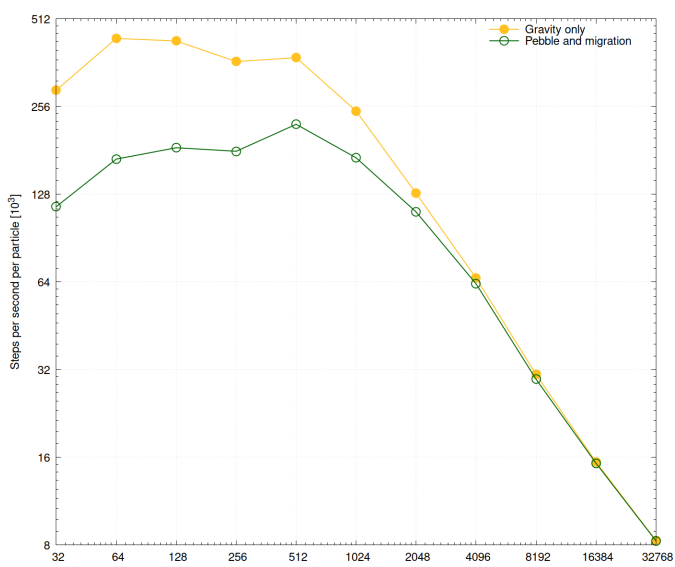


Figure 2: Speed of SyMBAp with 8 cores. The solid symbols are for gravity only and the open symbols are for the version used here that includes pebble accretion and planet migration. Simulations were run on AMD EPYC 7H12 CPUs with a clock speed of 3.0 GHz and compiled with GCC 13.2.

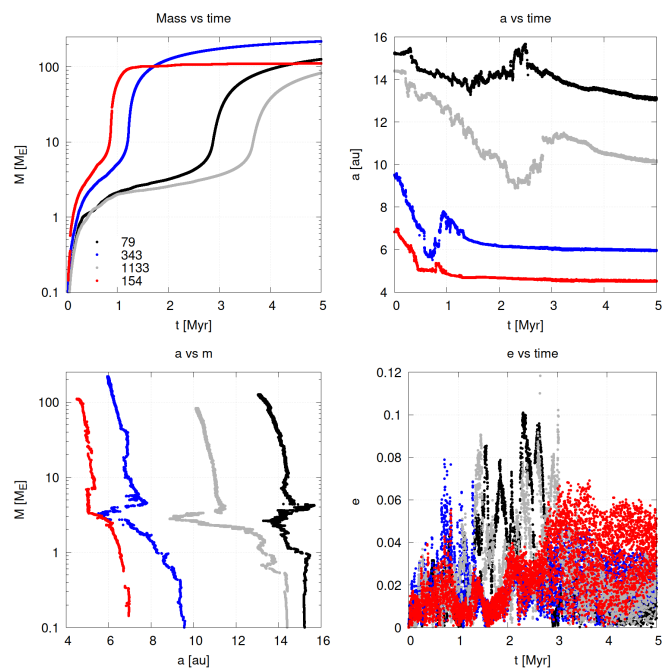


Figure 3: Truncated gas accretion due to the innermost planet being pushed into the cavity. The red (curve) planet is pushed into the cavity, inside 5 au and the gas accretion for it is halted

(2020). At present SyMBAp has no built-in mechanism to compute such a maximum and halt planet migration at the pressure maximum. Thus we opted for this crude approximation that halts planet migration at 5 au with the downside that there is no gas closer to the Sun even though the expectation is that the disc extended closer to the Sun.

As we mentioned in Section 3, we place a lunar-mass embryo near 5 au in the hope of triggering the formation of a Jupiter analogue (Brasser and Mojzsis, 2020). While the simulations were analysed, we became aware that we produced many Saturn analogues with final semi-major axes $a < 5$ au. These planets are situated in a region where no gas is present in the simulation. As a result, this embryo undergoes stunted growth because it settles at the inner edge of the disc, and then another planet that forms later slowly pushes it into the cavity while the planet is still accreting gas. This will eventually halt gas accretion and predominantly produce Saturn analogues inside the cavity. These analogues were not taken into account for the final results.

In Fig. 3, we show that this is indeed the case. This four-panel plot shows the evolution of mass vs. time (top left), semi-major axis vs time (top right), mass vs semi-major axis (bottom left) and eccentricity vs time (bottom right), for a system with four giant planets at the end. Each planet accretes mass at a different rate. The red curve shows the evolution of an embryo that starts near 7 au and then migrates inwards as it grows. After about 1.1 Myr, in the midst of rapidly accreting a gaseous envelope, the gas accretion stops. By this time, the said planet has reached the inner edge of the gas disc because it is pushed into the cavity by the second planet shown in blue; the pushing occurs because they are temporarily trapped in a 2:3 mean motion resonance. Gas accretion for the inner planet is halted while the mass of the outer planet keeps growing. The inner planet’s mass is stalled at $110 M_{\oplus}$ so that it qualifies as a Saturn analogue (see next subsection). After about 2.5 Myr and 3.5 Myr of evolution, two further planets undergo gas accretion and they end up with masses close to that of Saturn while the planet in blue ends up with a mass in between that of Jupiter and Saturn. The phenomenon of planets ending up inside the cavity and having their growth artificially halted is rather frequent, and is an artefact of our truncated gas disc at 5 au. Therefore from our results we have removed all giant planets whose final semi-major axis is less than 5 au.

4.2. Orbital distribution of giant planet analogues

The orbital distribution of giant planets at the end of the simulation shows significant variation among all the trials in terms of the number of giant planets, their orbital elements, the giant planet masses, and the remaining mass of planetesimals.

The orbital distribution of planets formed at the end of the simulation is shown in Fig. 4, which displays the $m_p - a$, $e - a$, and $m_p - e$ distributions for all planets in all simulations with $m_p > 10M_{\oplus}$ and $a > 5$ au. We chose a minimum giant planet mass of $10 M_{\oplus}$ because this is the approximate pebble

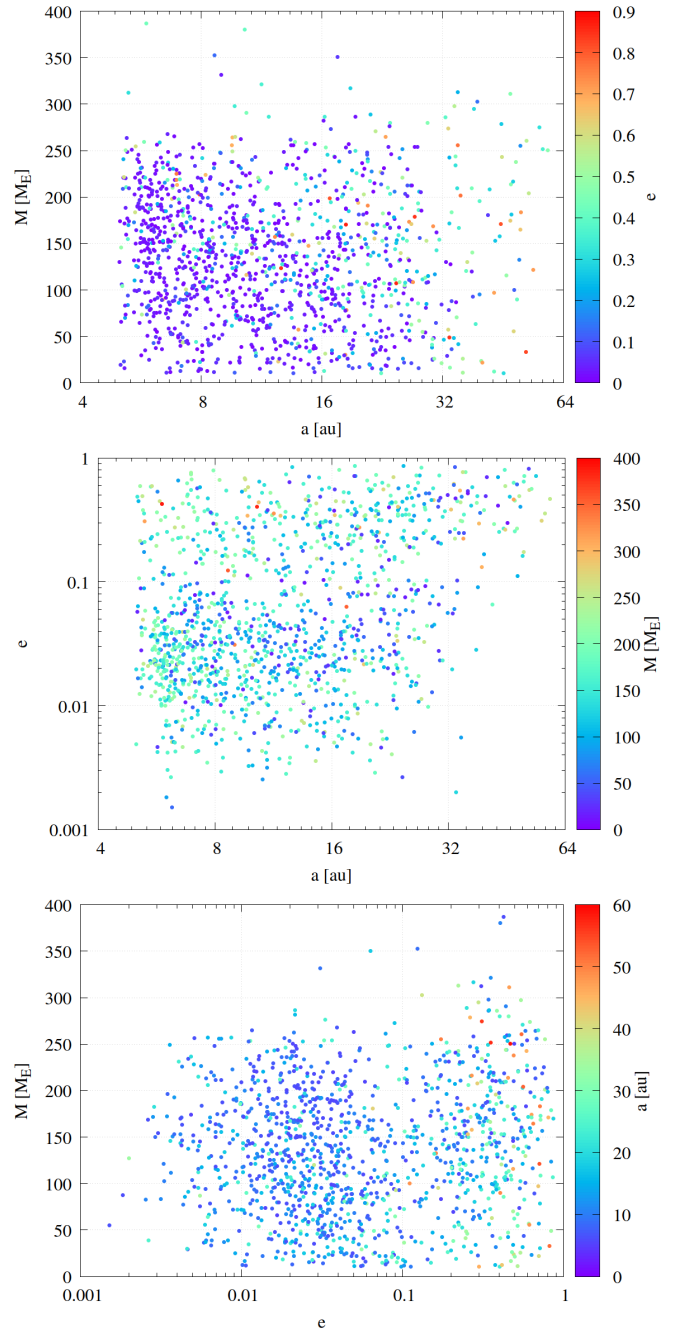


Figure 4: We show the distribution of giant planet mass, semi-major axis and eccentricity for all planets $m_p > 10M_{\oplus}$ over all simulations. The panels are: (a) $m_p - a$ (b) $e - a$ and (c) $m_p - e$. The colouring pertains to the un-plotted parameter (see the label next to the colorbar). Any correlation between these parameters is not seen.

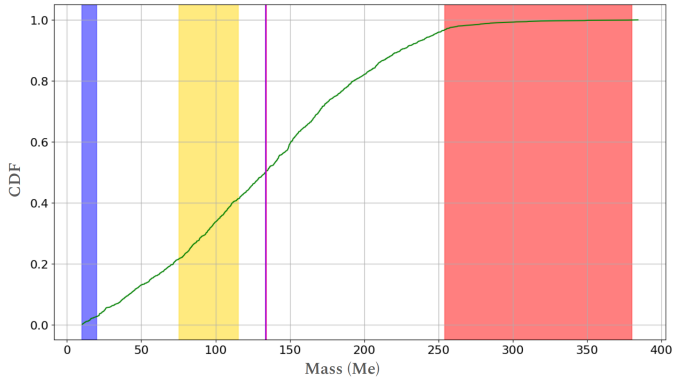


Figure 5: Cumulative distribution for the mass in planets with mass more massive than $10M_{\oplus}$ and $a \geq 5$ au. Both the mean and median mass in planets in each system is around $134 M_{\oplus}$. Blue, yellow and red vertical strips indicate range of ice giant, Saturn and Jupiter mass analogues range respectively.

isolation mass and from Fig. 3 we observe that gas envelope accretion starts roughly at this mass as well. In total we formed 1467 giant planets with mass $m_p > 10 M_{\oplus}$, of which 1158 have a semi-major axis $a > 5$ au, so that our outcomes are not constrained by low-number statistics. There appear to be few planets with a mass $m_p > 250 M_{\oplus}$ and, independently, with a semi-major axis $a \gtrsim 30$ au. The latter is not too surprising because we initially placed no planetesimals beyond 25 au. Most planets (66%) have low eccentricity $e < 0.1$. There appears to be no correlation between each of these three parameters. At the end of the simulations there are about 6% of planets with final eccentricities $e > 0.5$ and these are in dynamically unstable systems that have not yet fully evolved.

In the following, we define the mass range for Saturn analogues to be $75 - 115 M_{\oplus}$, $254 - 380 M_{\oplus}$ for Jupiter analogues and $10 - 20 M_{\oplus}$ for ice giant analogues. As shown in Fig. 5, after 5 Myr almost 50 % of the planet analogues formed have masses between $10 - 135 M_{\oplus}$, while 83 % have masses below $200 M_{\oplus}$. This implies that very few ice giant and Jupiter analogues are formed in the system, compared to Saturn analogues and planets with masses in between the ice giants and Saturn (I-S), and Saturn and Jupiter (S-J). Overall, 2.6% of giant planets are ice giant analogues, 17.8% are I-S analogues, 19.4% are Saturn analogues, 55.6% are S-J analogues and 4.4% are Jupiter analogues. The number of giant planets with $m_p > 10 M_{\oplus}$ at the end of the simulations is $\langle N \rangle = 1.83 \pm 1.24$.

In all simulations, we have not observed the formation of gas giants and ice giants in the same trial. We demonstrate this with a few figures. In Fig. 6 we show the final mass-semi major axis distribution of one set of simulations wherein we produce at least one Jupiter analogue in the entire set. It is clear that each system is unique, and that the mass in leftover planetesimals depends on the eccentricities of the giant planets at the time the simulations ended. We show the mass-semimajor axis evolution of one simulation producing a Saturn analogue with low eccentricity in Fig. 7. The colour coding is proportional to the eccentricity of each body.

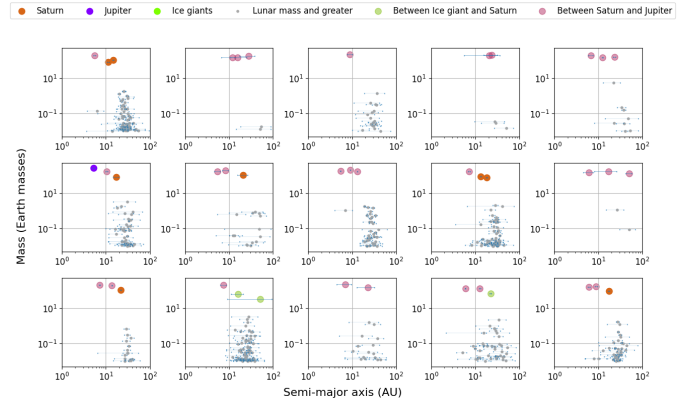


Figure 6: Final mass-semimajor axis distribution of a set of simulations with a system yielding both Jupiter and Saturn-mass planets. The middle-leftmost panel has both a Jupiter and a Saturn analogue. The horizontal error bars are a proxy for the eccentricity of the bodies. Parameters: $\text{peb_flg} = 1$, $\beta = 4.5$, $m_{\text{tot}} = 4$, $f = 1$ and $N = 1.5K$. For this f value it is difficult to form ice giants (discussed Section 4.3).

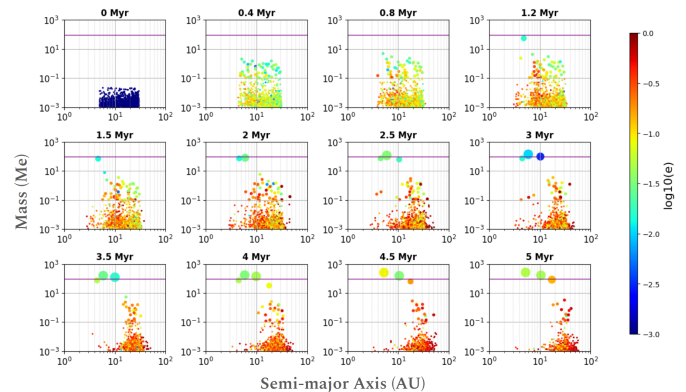


Figure 7: Snapshots of the mass and semi-major axis evolution of one simulation producing a Jupiter, Saturn and a SJ analogue. This is the same simulation as the middle leftmost panel in Fig. 6. The horizontal purple line indicates Saturn mass. The colour coding is a proxy for the eccentricity. High eccentricity values for left-over planetesimals indicate a dynamic system. This is the same simulation as shown in Fig. 18.

The cumulative distributions of semi-major axis and eccentricity for the five categories of giant planets are shown in Fig. 8. It appears that the Jupiter analogues are approximately evenly spaced in $\log a$, and the same is approximately true for the other types of giant planets, but there are intrinsic differences. The S-J planets are on average the most numerous and closest to the Sun (their median is 10.5 au) and the Jupiter analogues the farthest away (median 16.3 au). The cumulative eccentricity distribution may indicate why this is the case: the Jupiter analogues have, on average, the highest eccentricities, and the I-S planets the lowest. Only 33% of Jupiter analogues have an eccentricity $e < 0.1$ while this fraction is raised to 60% for the S-J planets and 70% for Saturn and I-S analogues. It turns out that systems that produce Jupiter analogues are dynamically less stable, leading to an episode of violent scattering. The median semi-major axis for Saturn analogues is 12.9 au, although it reduces to 10.8 au if we restrict ourselves

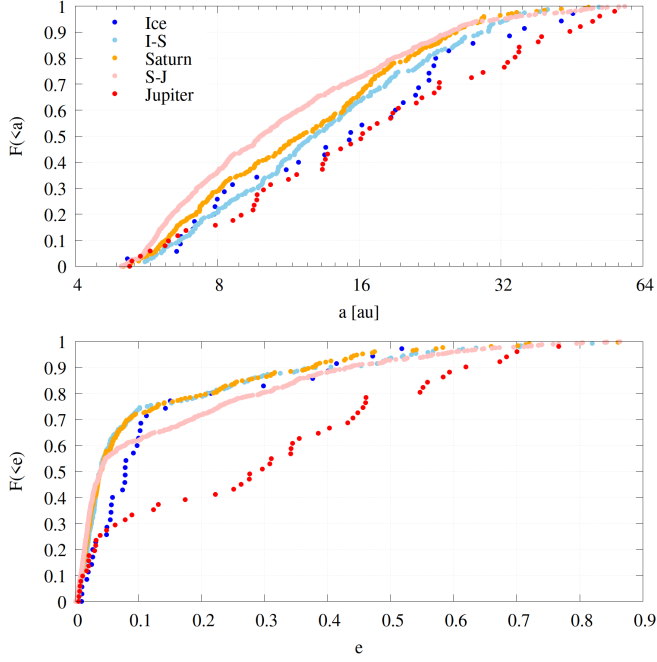


Figure 8: CDF distribution of (a) (b) e - a for all planets with $m_p > 10M_\oplus$ over all simulations. All the planets are approximately evenly placed in $\log a$. Jupiter analogues mostly have higher eccentricities than the other types.

to those Saturn analogues with $e < 0.1$. These results indicate that giant planets form throughout the disc with no strongly preferred location and mass configuration (see top panel of Fig. 4), and the outcome in terms of mass and semi-major axis appears random.

The higher eccentricity of Jupiter analogues than Saturn analogues is puzzling, but it is probably due to systems with Jupiter analogues having a lower final mass in planetesimals, which cannot damp the eccentricities of the Jupiter analogues. In Figure 9 we plot snapshots of the evolution of a simulation that produces a single Jupiter analogue on an eccentric orbit. The eccentricity of the giant planets increases due to their mutual scattering, and remains high once the planetesimals are almost completely removed from the system around 3.5 Myr. We back up our claim by showing the final fraction of planetesimals remaining in the simulations versus mean giant planet mass in Fig. 10. We see a rapidly decreasing trend for the fraction of left-over planetesimals, with individual mass less than a lunar mass, with increasing giant planet mass. In other words: the higher the mean mass of giant planets in each simulation, the lower is the fraction of planetesimals remaining.

In Fig. 11 we plot the mass in solids – from pebble accretion – versus the mass in gas for the five types of giant planet that we form. The respective fractions of the planetary masses in solids and gas are 0.19 ± 0.05 for the ice giants, 0.06 ± 0.02 for I-S giants, 0.04 ± 0.01 for Saturn analogues, and 0.02 ± 0.007 for both S-J and Jupiter analogues. We further computed that planets with a mass of about $4 M_\oplus$ have a roughly equal

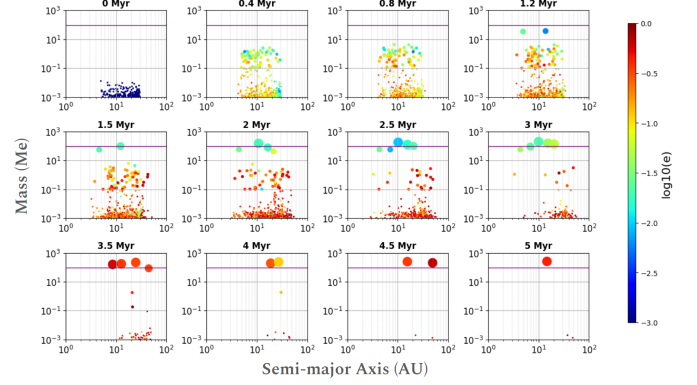


Figure 9: Snapshots of the mass and semi-major axis evolution of one simulation forming an eccentric Jupiter. The horizontal purple line indicates Saturn mass. The colour coding is a proxy for the eccentricity. This is the same case as shown in Fig. 14. There are hardly any planetesimals left at the end of 5 Myrs.

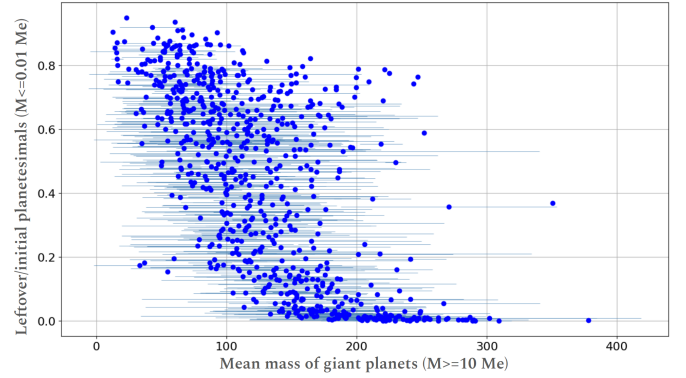


Figure 10: Fraction of leftover planetesimals (vertical) versus the mean mass in giant planets ($M > 10M_\oplus$)(horizontal). The normalisation for the vertical axis is done with the initial number of planetesimals for that system. The uncertainty is the standard deviation in giant planet mass. Each dot represents a the mean of giant planet mass from a single simulation. We see an inverse trend for the left-over planetesimals with increasing mass.

mass in core and envelope, consistent with the simulations of Matsumura et al. (2021).

4.3. Input parameter dependence

We calculate the success of forming some giant planet analogue through the parameter λ , which is the number of giant planet analogues per run, and is calculated as

$$\lambda = \frac{\text{Total number of planets formed in all runs}}{\text{Total number of runs}} \quad (33)$$

This is evaluated for Jupiter, S-J, Saturn, I-S and ice giant analogues. In this section, we will show which values of parameters have the highest success chance in forming Saturn analogues, and also give the best combination of parameters that best reproduces the overall outer solar system. Even though the pebble accretion prescription of Ormel and Liu (2018) is an improvement over that of Ida et al. (2016), we prefer to show the results of both prescriptions.

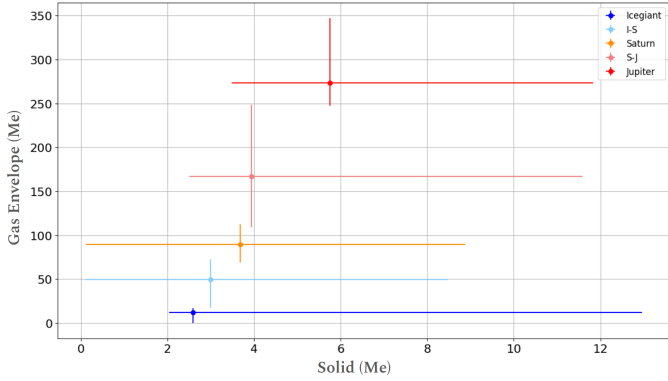


Figure 11: Mass in solids (horizontal) versus mass in gas (vertical) for the five different types of giant planets. The means are plotted. The uncertainties are the min and max values.

The fraction of obtaining a Saturn analogue with the Ida pebble accretion prescription is 0.33 ± 0.26 (σ) while with the Ormel prescription this is 0.32 ± 0.17 , which are statistically identical. These fractions are 0.19 ± 0.16 when the sticking efficiency $f = 0.5$, 0.38 ± 0.2 when $f = 0.75$ and 0.35 ± 0.24 when $f = 1$. These values are also identical within uncertainties. Concerning the initial total mass in planetesimals, then fractions are 0.21 ± 0.21 when $m_{\text{tot}} = 0.5 M_{\oplus}$, 0.33 ± 0.17 when $m_{\text{tot}} = 1 M_{\oplus}$ and 0.34 ± 0.25 when $m_{\text{tot}} = 4 M_{\oplus}$.

In contrast, the fraction for forming Jupiter analogues is strongly dependent on the pebble accretion prescription used. With the Ida prescription the fraction is 0.11 ± 0.26 , while with Ormel’s prescription the fraction for forming Jupiter analogues is 0.02 ± 0.03 , which is substantially different. Similarly the sticking efficiency plays an important role in the production of Jupiter analogues: when $f = 0.5$, we produce no Jupiter analogues because the growth is too slow. When this is increased to $f = 0.75$, the fraction increases to 0.02 ± 0.06 , but it jumps to 0.17 ± 0.29 when $f = 1$. Overall the likelihood of obtaining Jupiter analogues and massive gas giants, with mass in between Saturn and Jupiter, decreases with the more detailed accretion efficiency model by Ormel and Liu (2018) and lower sticking efficiency.

This dependence of the average number of Saturn analogues (and other mass analogues) on different parameter values can be seen in the scatter plots (Fig. 12). To check whether different values of the same parameter significantly affect the probability of Saturn analogue formation, we ran the K-sample Anderson-Darling test (Anderson & Darling, 1952) for all possible parameter combinations. This test checks whether several collections of observations can be modelled as coming from a single population, and where the distribution function does not have to be specified. It is more sensitive at the tail ends of the distribution than the Komolgorov-Smirnov test. To eliminate strong statistical biases we have only tested those parameters for which we have more than ten sets of simulations. These parameters are: $m_{\text{disc}} = 1$ and $4 M_{\oplus}$, and $N = 1000$ and 1500 , and all other values of the pebble accretion

prescription, f , and β . We found only a few combination of parameters where the p -value of the λ distribution was below 5% for Saturn analogues, suggesting that no single parameter has a dominant effect on the efficiency of Saturn analogue formation. In other words, the distribution of outcomes are not statistically different when adopting different input parameters e.g. the outcomes with the Ormel and Ida prescriptions, or the initial slope of distribution. The only combinations that yielded $p < 0.05$ are with $f = 0.5$ and 0.75 , and $N = 1000$, and 1500 . For Jupiter and ice giant analogues there are too few outcomes that have $\lambda > 0$, so that the outcome of the Anderson-Darling and K-S tests is not very meaningful. Yet, from Figure 12 and looking at S-J analogues, we see that Ida’s prescription and $f = 1$ tend to form more massive planets, leaning towards Jupiter-mass analogues. Conversely, Ormel’s prescription with $f = 1$ decreases the formation efficiency of ice giants and I-S analogues, while $m_{\text{tot}} = 4 M_{\oplus}$ somewhat favours their formation. A slightly significant trend is seen with the number of planetesimals N . With $N = 1000$ and 1500 , the number of planets produced increase with their mass. Overall the sticking efficiency f has the most significant effect on the likelihood of forming different types of planet analogues, because in essence it is another parameterisation of the pebble flux.

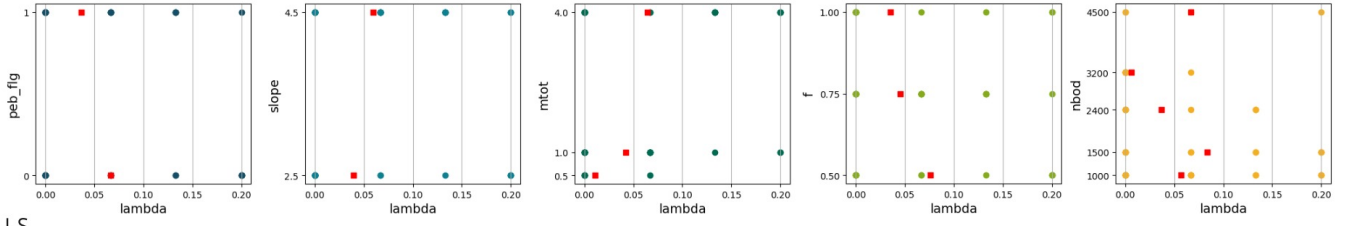
Figure 13 summarises the likelihood of forming different planets for different parameter combination. Although we do not find one single most significant parameter, the chart is sorted according to the most sensitive parameter, f , followed by the pebble accretion prescription and the initial number of bodies, N .

4.4. Gas giant growth time distribution

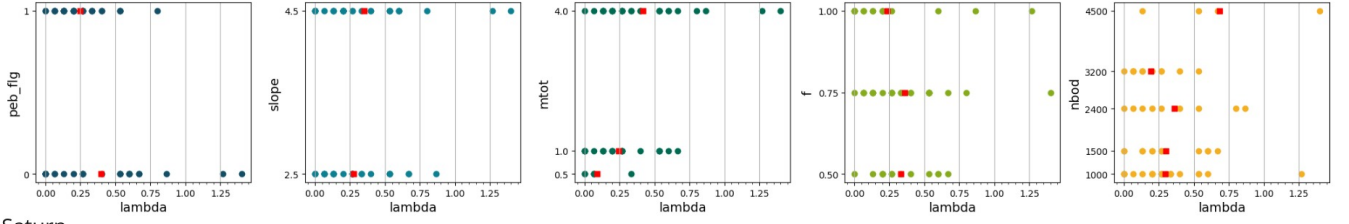
In this subsection, we analyse the time of formation for all types of gas giants. Fig. 14 tracks the growth of planets in mass over 5 Myr for a semi-major axis that is close to the mean value for each type of planet. All the planets start from embryos with mass $\leq 0.01 M_{\oplus}$ which grow to $1 M_{\oplus}$ within 0.4 Myrs. After this time the growth rate for some bodies slows down considerably. The figure shows that the planets reach $10 M_{\oplus}$ cores in a sequential manner: Jupiter analogue cores form by 1 Myr while ice giant analogue cores form the last at around 4.8 Myrs.

We calculate the time it takes each giant planet to reach $10 M_{\oplus}$. There are several reasons for us doing so. First, because it was traditionally considered to be a problem to reach this mass from planetesimal accretion within the disc’s lifetime in this region of the Solar System (Pollack et al., 1996). Pebble accretion has clearly alleviated this problem. In addition, the average pebble isolation mass across the giant planet region is about $10 M_{\oplus}$ and Fig. 11 shows that $10 M_{\oplus}$ is also the approximate upper mass at which gas accretion sets in. The pebble isolation mass is thought to be the mass at which the planet creates wakes in the disc that halt further accretion (Lambrechts et al., 2014), and a successful link has been made between the core formation time of Jupiter and the radiometric Hf-W ages of iron

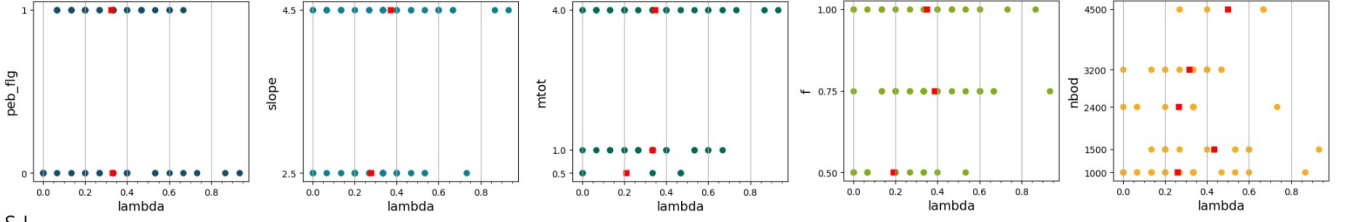
(a) Ice giant



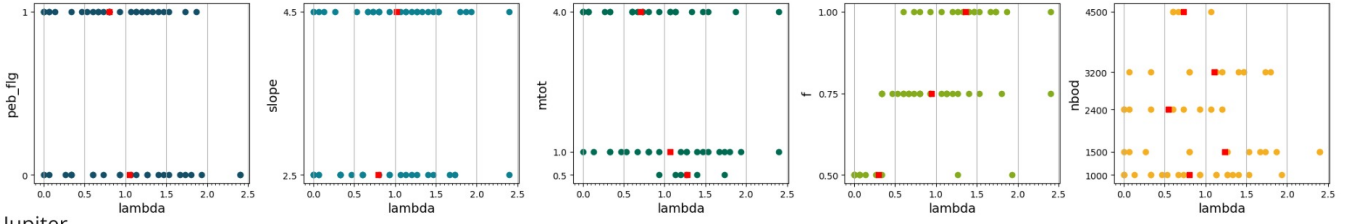
(b) I-S



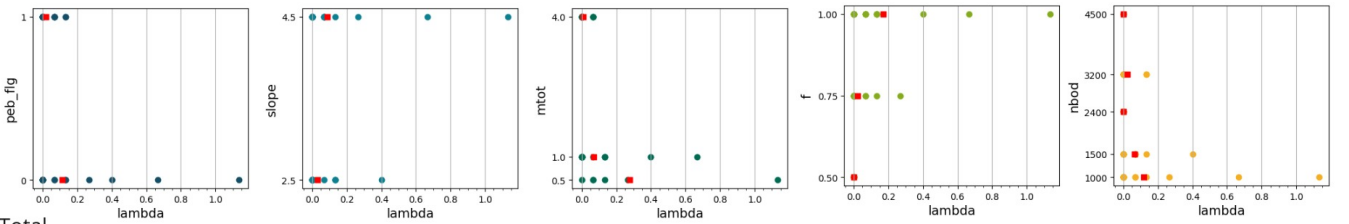
(c) Saturn



(d) S-J



(e) Jupiter



(f) Total

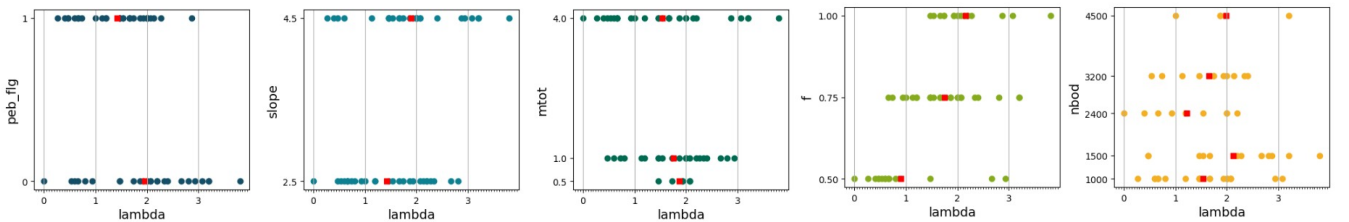


Figure 12: Scatter plot for different parameter values vs λ from (a) Ice giants to (e) Jupiter mass analogues and (f) all massive bodies. Here for each parameter value, the values of other parameters are varying. The red square indicates the mean of the distribution. There is no single parameter that stands out for any planets formation. Please note that the x-axis limits are varying.

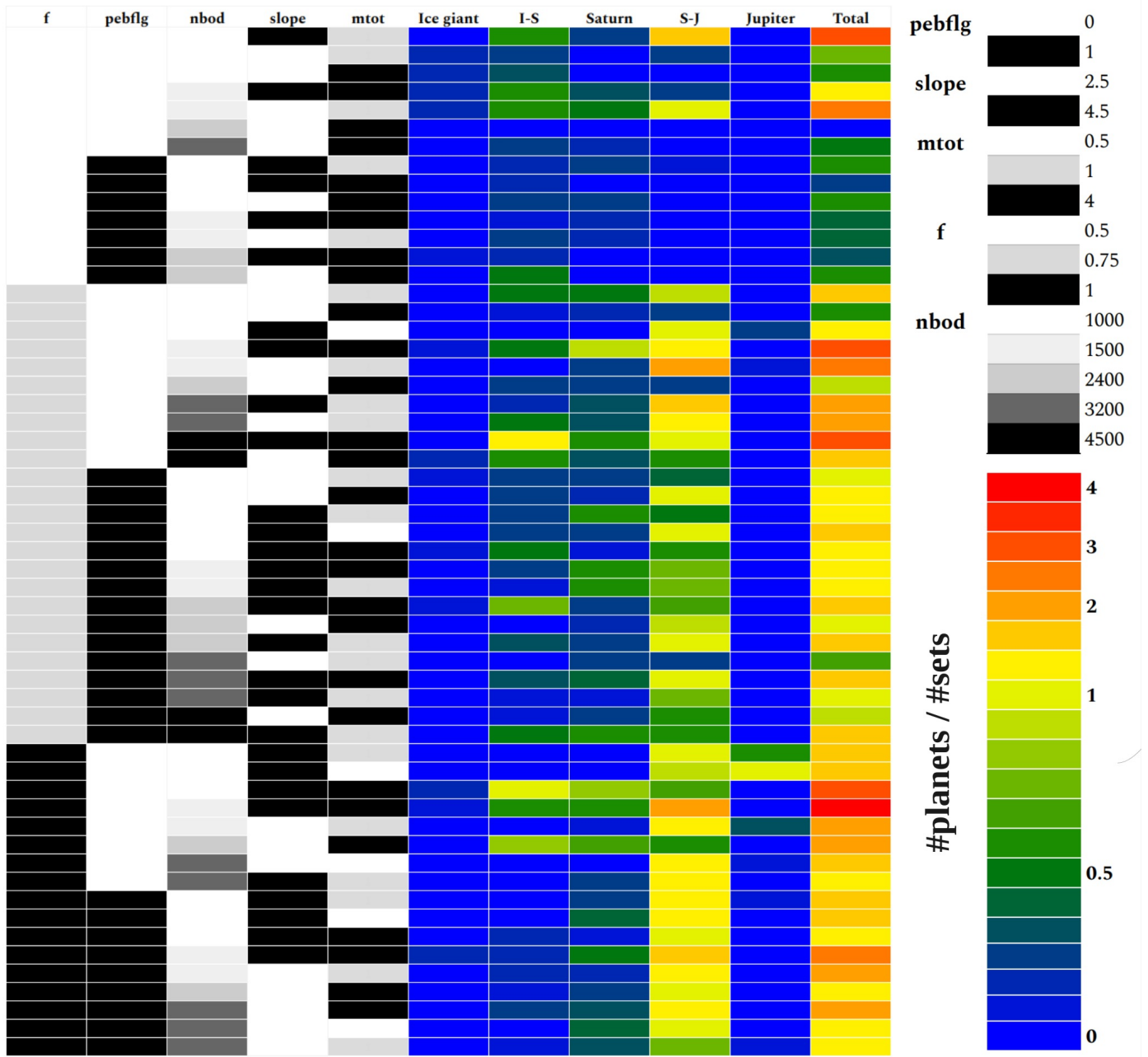


Figure 13: Summary of all the parameter combinations and their respective λ values for each planet. The chart is sorted according to f , followed by $peb.flg$ and N . The color bar is deliberately non-uniformly colored to enhance comprehension of the likelihood distribution across the range of values spanning from 0 to 1.

meteorites (Kruijer et al., 2017). Here we build on these results.

In Fig. 15 we show a cumulative distribution of the time it takes for a planetesimal to grow to $10 M_{\oplus}$ that will eventually end up as one of the various kind of giant planets. The Jupiter analogues grow the fastest, reaching $10 M_{\oplus}$ in $\langle t_{c,J} \rangle = 1.1 \pm 0.3$ Myr. For Saturn analogues this takes considerably longer: $\langle t_{c,S} \rangle = 3.3 \pm 0.4$ Myr, and for the ice giants it takes $\langle t_{c,I} \rangle = 4.9 \pm 0.1$ Myr. These results indicate that the three types of giant planet in the Solar System formed at distinct, non-overlapping times. The two other types of giant planet, not present in the Solar System, have mean core growth times of $\langle t_{c,SJ} \rangle = 2.0 \pm 0.6$ Myr and $\langle t_{c,IS} \rangle = 4.3 \pm 0.4$ Myr. In summary: the cores of the giant planets of the Solar System formed in sequence.

The final mass attained by a planet core with a mass of $10 M_{\oplus}$ as a function of its formation time was also examined, and is illustrated in Fig. 16. The figure reveals a roughly linear inverse relationship, albeit with large scatter when $t \lesssim 2$ Myr, between the accretion time and the final mass achieved by a $10 M_{\oplus}$ core. Faster core formation results in a more massive planet after 5 Myr.

Last, we investigated how long it takes for the Saturn analogues to reach $75 M_{\oplus}$ and the Jupiter analogues to reach $254 M_{\oplus}$. This is shown in Fig. 17, where we plot the time that it takes after core formation for Jupiter and Saturn analogues to reach 80% of their mass. The Saturn analogues reached 80% of their final mass much faster than the Jupiter analogues. Indeed, the Saturn analogues reach $75 M_{\oplus}$ in $\langle t_{gas,S} \rangle = 0.64 \pm 0.33$ Myr after core formation, while for Jupiter it takes $\langle t_{gas,J} \rangle = 3.37 \pm 0.45$ Myr. Saturn’s core forms later, but it finishes growing at more or less the same time as Jupiter. Both planets reach their final masses in 4 to 4.5 Myr, which is about the time the disc is thought to have dispersed (Wang et al., 2017).

In summary, our results indicate that the giant planets in the Solar System could have formed sequentially, with the Jupiter analogues forming first, and ice giants only arising at the very end of the simulation, with a formation time very close to 5 Myr, and Saturn analogues are formed from $10 M_{\oplus}$ cores after 3 Myr.

5. Discussion

At the end of the simulations we have many Mars- and Earth-mass bodies. These bodies do not appear in the current Solar System so they need to be removed from the simulations at some point in time. Most of these will be ejected once the simulations are carried on for longer, and many of them have already been removed in the more violent simulations. The long term evolution of these simulations will be investigated in a separate publication.

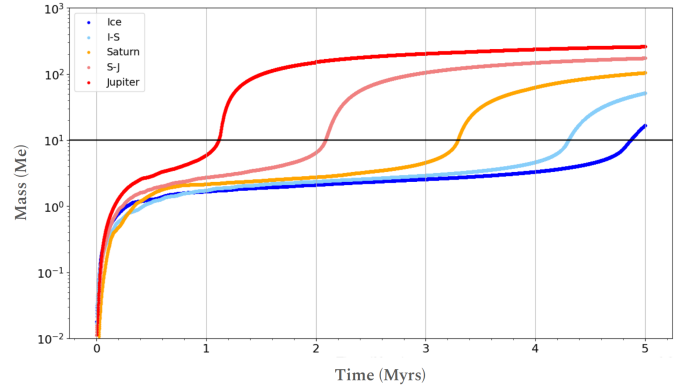


Figure 14: Tracking growth of all the 5 types of planets over 5 Myr with their typical core formation times. The semi-major axes of each case was close to the mean value for that specific kind of planet. Sequential core formation is discernible.

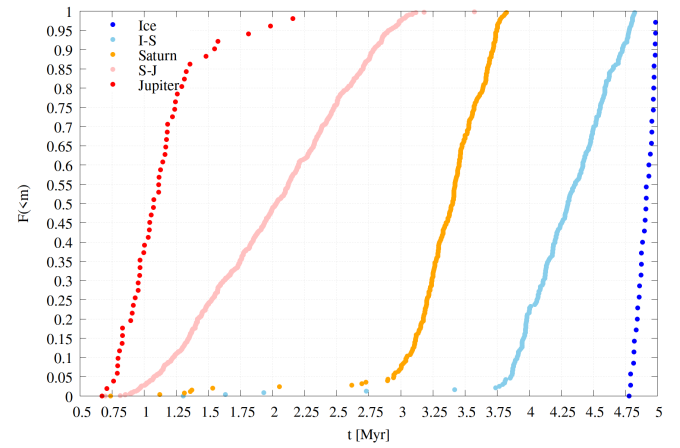


Figure 15: Cumulative distribution for time of accretion to form $10 M_{\oplus}$ cores for all five different giant planet analogues. The planets form in distinct time intervals.

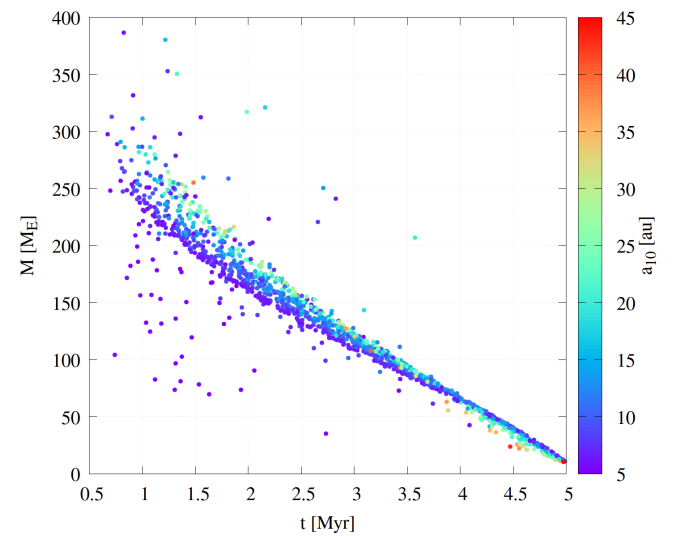


Figure 16: Final mass reached at 5 Myr vs time of accretion to form $10 M_{\oplus}$. Colours indicates the semi-major axis at which the planet core formed. An inverse relationship is seen.

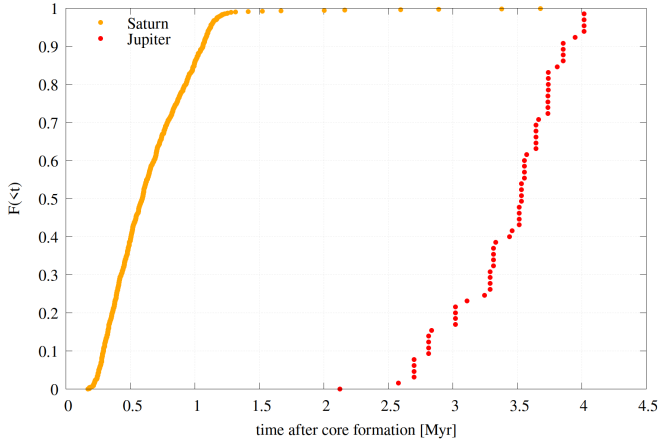


Figure 17: Cumulative time distribution after core formation for the Saturn and Jupiter analogues to reach 80% of their current mass. While Saturn reaches 80% of its mass after core formation faster than Jupiter, both planets reach their final masses around the same absolute time.

5.1. Jupiter analogues with a high semi-major axis

We observed the formation of Jupiter analogues as far as 16.3 au from the Sun, which is on average farther than the Saturn analogues (see Fig. 8). As suggested by Thommes et al. (1999), giant planets in compact arrangements may undergo a dynamical instability, thereby augmenting their eccentricities. Thommes et al. (2008) showed that Jupiter and Saturn can swap their orbits, so that it is not necessary to have Jupiter form inside of Saturn.

5.2. Comparison with chronology from the meteorite record

Here we briefly discuss how our simulations compare with the cosmochemical meteorite record. A more in-depth analysis is done in a separate publication.

Our numerical results indicate that the gas giants have almost fully formed by about 4 Myr after the start of the simulations. By itself this is interesting, but ideally the model should be anchored to chronological data from the meteorite record. Is there any such evidence that supports or invalidates our model?

From our simulations, the time it takes for the formation of Jupiter’s core is comparable to the time taken as inferred from ^{182}Hf - ^{182}W systematics and modelled accretion ages of the various meteorite types (i.e., non-carbonaceous and carbonaceous) of iron meteorite parent bodies Kruijer et al. (2017). In contrast, Johnson et al. (2016) suggested that the growth of Jupiter is reflected in the timing of the impact resetting of the chondrules of the CB (Bencubbin-like) carbonaceous chondrites, which occurred around ~ 5 Myr after CAIs (Krot et al., 2005). This timing was however revised recently from ^{182}Hf - ^{182}W compositions of CH and CB chondrites that indicate that the impact occurred at 3.8 ± 0.8 Myr after the formation of Ca-Al-rich Inclusions (CAIs) (Wölfer et al., 2023). The formation of CB, CH, and CR chondrite parent

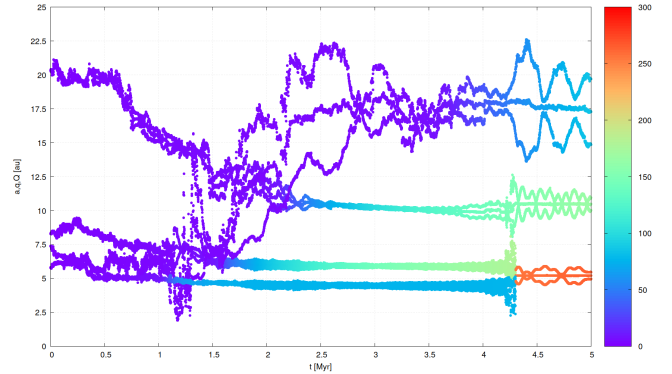


Figure 18: Evolution of the system displayed in the leftmost middle panel of Fig. 6. This system yields both a Saturn and a Jupiter-mass planet. The Jupiter analogue is the result of a merger near 4 Myr and 5 au.

bodies therefore took place up to ~ 1 Myr earlier than previously proposed based on Pb-Pb chronology of CB chondrules (Krot et al., 2005; Bollard et al., 2015). However, the core of our Jupiter analogues formed much earlier, and our Jupiter analogues have reached a mass of approximately $250 M_{\oplus}$ after 3.8 Myr. As such, our simulations align better with the suggestions of Kruijer et al. (2017) that the separation of the NC and CC reservoirs, as constrained from accretion ages of iron meteorite parent bodies, may correspond to the formation of Jupiter core. The later 3.8 Myr metal-silicate fractionation age recorded in CB, CH and CR chondrites may be associated with other high-velocity impact events in the outer solar system.

For the Jupiter analogues the most important free parameter is the initial mass in planetesimals, probably because there are more high-mass planetesimals in the disc that can rapidly accrete pebbles and enter a runaway growth phase. There is an increased role for the different pebble accretion prescriptions for Jupiter, and the best parameters for producing Jupiter analogues are Ida’s pebble accretion prescription, number of planetesimals $N = 1500$, and sticking efficiency $f = 1$. These parameters tend towards optimisation for the fastest possible growth. For these parameter combinations Jupiter’s growth is consistent with that advocated by Kruijer et al. (2017).

6. Summary and conclusions

This study investigates the formation and evolution of giant planets through N-body simulations using the parallel version of SyMBA (Lau and Lee, 2023). The simulations include damping forces from the gas disc, pebble and gas-envelope accretion, and various parameter values to replicate realistic conditions. A total of 840 simulations were conducted with different parameter combinations, initially focused on understanding Saturn’s formation, but ultimately to understand giant planet formation as a whole. The simulations ran for 5 million years, tracking the dynamics of self-gravitating planetesimals. The computational efficiency of the simulations, orbital distribution, core formation time and parameter combinations were systematically tested and analyzed. Key parameters studied

include sticking efficiency, pebble accretion prescription, initial total planetesimal mass, size-frequency slope, and the initial number of planetesimals.

At the end of 5 Myr, while we observed a significant diversity in the orbital distribution of giant planets, we saw no correlation between semi-major axis, eccentricity and mass of the planet. Apart from Jupiter analogues, most giant planets exhibit low eccentricities ($e < 0.1$), with a small fraction displaying eccentricities exceeding 0.5, indicative of dynamically unstable systems. The cumulative distributions of semi-major axis and eccentricity highlight differences among planet types; however, there is no preferred location or mass configuration for the giant planet formation. Jupiter analogues are on average much more eccentric, possibly due to dynamical instabilities that leave too little mass in planetesimals to damp the eccentricities down.

The likelihood of forming a type of planet (λ) analogues varied based on parameter combinations. Statistical tests suggest no single parameter significantly dominates formation efficiency, indicating a complex interplay among parameters. Nonetheless, the sticking efficiency appears to have the most significant impact on the formation of different types of planet analogues, but not at a 2σ level.

Finally, we analyzed the mean formation times of the cores of the giant planet analogues. Jupiter analogues exhibit the shortest growth time (to grow into $10 M_{\oplus}$), with a mean of $\langle t_{c,J} \rangle = 1.1 \pm 0.3$ Myr, followed by Saturn analogues $\langle t_{c,S} \rangle = 3.3 \pm 0.4$ Myr and ice giants $\langle t_{c,I} \rangle = 4.9 \pm 0.1$ Myr, indicating sequential formation. Additionally, we observe that the final mass attained by a $10 M_{\oplus}$ core is inversely proportional to its formation time, reinforcing the notion of sequential formation in the solar system. Furthermore, we explore the time taken for Saturn analogues to reach $75 M_{\oplus}$ and Jupiter analogues to reach $254 M_{\oplus}$, finding that Saturn analogues reach 80 % of their final mass earlier than Jupiter analogues, though both reach their final masses in 4 to 4.5 Myr, aligning with the estimated dispersal time of the disc.

Our findings provide valuable insights into the timing and mechanisms of giant planet formation, offering implications for our understanding of the early solar system dynamics as well as shortcomings and possibilities for improvement. In the future, we will focus on achieving the formation of Jupiter and Saturn with their current orbital configurations. We aim to explore the intricate substructures of protoplanetary discs, such as rings, in order to better understand their influence on the formation and positioning of these gas giants in the solar system.

Acknowledgements

T.C.H.L. acknowledges funding from the Deutsche Forschungsgemeinschaft (DFG, German Research Foundation) under grant 325594231. We thank Sourav Chatterjee for useful comments.

References

- Ataiee, S., Baruteau, C., Alibert, Y., Benz, W., 2018. How much does turbulence change the pebble isolation mass for planet formation? *Astronomy and Astrophysics* 615, A110. doi:10.1051/0004-6361/201732026.
- Bai, X.N., 2017. Global Simulations of the Inner Regions of Protoplanetary Disks with Comprehensive Disk Microphysics. *The Astrophysical Journal* 845, 75. doi:10.3847/1538-4357/aa7dda.
- Bitsch, B., Izidoro, A., Johansen, A., Raymond, S.N., Morbidelli, A., Lambrechts, M., Jacobson, S.A., 2019. Formation of planetary systems by pebble accretion and migration: growth of gas giants. *Astronomy and Astrophysics* 623, A88. doi:10.1051/0004-6361/201834489.
- Blum, J., Wurm, G., 2000. Experiments on Sticking, Restructuring, and Fragmentation of Protoplanetary Dust Aggregates. *Icarus* 143, 138–146. doi:10.1006/icar.1999.6234.
- Bollard, J., Connelly, J.N., Bizzarro, M., 2015. Pb-Pb dating of individual chondrules from the CB_a chondrite Gajba: Assessment of the impact plume formation model. *The Meteoritical Society* 50, 1197–1216. doi:10.1111/maps.12461.
- Brasser, R., Mojzsis, S.J., 2020. The partitioning of the inner and outer Solar System by a structured protoplanetary disk. *Nature Astronomy* 4, 492–499. doi:10.1038/s41550-019-0978-6.
- Carrera, D., Gorti, U., Johansen, A., Davies, M.B., 2017. Planetesimal formation by the streaming instability in a photoevaporating disk. *The Astrophysical Journal* 839, 16.
- Carrera, D., Johansen, A., Davies, M.B., 2015. How to form planetesimals from mm-sized chondrules and chondrule aggregates. *Astronomy and Astrophysics* 579.
- Cuzzi, J.N., Hogan, R.C., Shariff, K., 2008. Toward Planetesimals: Dense Chondrule Clumps in the Protoplanetary Nebula. *The Astrophysical Journal* 687, 1432–1447. doi:10.1086/591239.
- Dohnanyi, J., 1969. Collisional model of asteroids and their debris. *Journal of Geophysical Research* 74, 2531–2554.
- Drążkowska, J., Alibert, Y., Moore, B., 2016. Close-in planetesimal formation by pile-up of drifting pebbles. *A&A* 594.
- Duncan, M.J., Levison, H.F., Lee, M.H., 1998. A Multiple Time Step Symplectic Algorithm for Integrating Close Encounters. *The Astronomical Journal* 116, 2067–2077. doi:10.1086/300541.
- Fendyke, S.M., Nelson, R.P., 2014. On the corotation torque for low-mass eccentric planets. *Monthly Notices of the Royal Astronomical Society* 437, 96–107. doi:10.1093/mnras/stt1867.
- Gerbig, K., Li, R., 2023. Planetesimal initial mass functions following diffusion-regulated gravitational collapse. *The Astrophysical Journal* 949, 81. URL: <https://dx.doi.org/10.3847/1538-4357/acca1a>.
- Goldreich, P., Ward, W.R., 1973. The Formation of Planetesimals. *The Astrophysical Journal* 183, 1051–1062. doi:10.1086/152291.
- Hartmann, L., Calvet, N., Gullbring, E., D’Alessio, P., 1998. Accretion and the Evolution of T Tauri Disks. *The Astrophysical Journal* 495, 385–400. doi:10.1086/305277.
- Ida, S., Guillot, T., Morbidelli, A., 2016. The radial dependence of pebble accretion rates: A source of diversity in planetary systems. I. Analytical formulation. *Astronomy and Astrophysics* 591, A72. doi:10.1051/0004-6361/201628099.
- Ida, S., Muto, T., Matsumura, S., Brasser, R., 2020. A new and simple prescription for planet orbital migration and eccentricity damping by planet-disc interactions based on dynamical friction. *Monthly Notices of the Royal Astronomical Society* 494, 5666–5674. doi:10.1093/mnras/staa1073.
- Ida, S., Tanaka, H., Johansen, A., Kanagawa, K.D., Tanigawa, T., 2018. Slowing Down Type II Migration of Gas Giants to Match Observational Data. *The Astrophysical Journal* 864, 77. doi:10.3847/1538-4357/aad69c.
- Ida, S., Yamamura, T., Okuzumi, S., 2019. Water delivery by pebble accretion to rocky planets in habitable zones in evolving disks. *Astronomy and Astrophysics* 624, A28. doi:10.1051/0004-6361/201834556.
- Ikoma, M., Nakazawa, K., Emori, H., 2000. Formation of Giant Planets: Dependences on Core Accretion Rate and Grain Opacity. *The Astrophysical Journal* 537, 1013–1025. doi:10.1086/309050.
- Johansen, A., Lacerda, P., 2010. Prograde rotation of protoplanets by accretion of pebbles in a gaseous environment. *Monthly Notices of the Royal Astronomical Society* 404, 475–485. doi:10.1111/j.1365-2966.2010.16309.x.
- Johansen, A., Mac Low, M.M., Lacerda, P., Bizzarro, M., 2015. Growth of as-

- teroids, planetary embryos, and Kuiper belt objects by chondrule accretion. *Science Advances* 1, 1500109. doi:10.1126/sciadv.1500109.
- Johansen, A., Oishi, J.S., Mac Low, M.M., Klahr, H., Henning, T., Youdin, A., 2007. Rapid planetesimal formation in turbulent circumstellar disks. *Nature Astronomy* 448, 1022–1025. doi:10.1038/nature06086.
- Johnson, B.C., Blair, D.M., Collins, G.S., Melosh, H.J., Freed, A.M., Taylor, G.J., Head, J.W., Wiczorek, M.A., Andrews-Hanna, J.C., Nimmo, F., et al., 2016. Formation of the orientale lunar multiring basin. *Science* 354, 441–444.
- Kanagawa, K.D., Tanaka, H., Szuskiewicz, E., 2018. Radial Migration of Gap-opening Planets in Protoplanetary Disks. I. The Case of a Single Planet. *The Astrophysical Journal* 861, 140. doi:10.3847/1538-4357/aac8d9.
- Krot, A.N., Amelin, Y., Cassen, P., Meibom, A., 2005. Young chondrules in CB chondrites from a giant impact in the early Solar System. *Nature Astronomy* 436, 989–992. doi:10.1038/nature03830.
- Kruijer, T.S., Burkhardt, C., Budde, G., Kleine, T., 2017. Age of Jupiter inferred from the distinct genetics and formation times of meteorites. *Proceedings of the National Academy of Science* 114, 6712–6716. doi:10.1073/pnas.1704461114.
- Lambrechts, M., Johansen, A., 2012. Rapid growth of gas-giant cores by pebble accretion. *Astronomy and Astrophysics* 544, A32. doi:10.1051/0004-6361/201219127.
- Lambrechts, M., Johansen, A., 2014. Forming the cores of giant planets from the radial pebble flux in protoplanetary discs. *Astronomy and Astrophysics* 572, A107. doi:10.1051/0004-6361/201424343.
- Lambrechts, M., Johansen, A., Morbidelli, A., 2014. Separating gas-giant and ice-giant planets by halting pebble accretion. *Astronomy and Astrophysics* 572, A35. doi:10.1051/0004-6361/201423814.
- Lau, T.C.H., Lee, M.H., 2023. Parallelization of the Symplectic Massive Body Algorithm (SyMBA) N-body Code. *Research Notes of the American Astronomical Society* 7, 74. doi:10.3847/2515-5172/accc8a.
- Lau, T.C.H., Lee, M.H., Brasser, R., Matsumura, S., 2024. Can the giant planets of the Solar System form via pebble accretion in a smooth protoplanetary disc? *arXiv e-prints* doi:10.48550/arXiv.2401.05036, arXiv:2401.05036.
- Lenz, C.T., Klahr, H., Birnstiel, T., 2019. Planetesimal population synthesis: Pebble flux-regulated planetesimal formation. *The Astrophysical Journal* 874, 36.
- Lenz, C.T., Klahr, H., Birnstiel, T., Kretke, K., Stammler, S., 2020. Constraining the parameter space for the solar nebula. *Astronomy and Astrophysics* 640.
- Levison, H.F., Kretke, K.A., Duncan, M.J., 2015. Growing the gas-giant planets by the gradual accumulation of pebbles. *Nature* 524, 322–324. doi:10.1038/nature14675.
- Levison, H.F., Thommes, E., Duncan, M.J., 2010. Modeling the Formation of Giant Planet Cores. I. Evaluating Key Processes. *The Astronomical Journal* 139, 1297–1314. doi:10.1088/0004-6256/139/4/1297.
- Li, R., Youdin, A.N., 2021. Thresholds for particle clumping by the streaming instability. *The Astrophysical Journal* 919, 107.
- Lynden-Bell, D., Pringle, J.E., 1974. The evolution of viscous discs and the origin of the nebular variables. *Monthly Notices of the Royal Astronomical Society* 168, 603–637.
- Mamajek, E.E., 2009. Initial conditions of planet formation: lifetimes of primordial disks, in: *AIP Conference Proceedings*, American Institute of Physics, pp. 3–10.
- Manara, C.F., Fedele, D., Herczeg, G.J., Teixeira, P.S., 2016. X-Shooter study of accretion in Chamaeleon I. *Astronomy and Astrophysics* 585, A136. doi:10.1051/0004-6361/201527224.
- Matsumura, S., Brasser, R., Ida, S., 2017. N-body simulations of planet formation via pebble accretion. I. First results. *Astronomy and Astrophysics* 607, A67. doi:10.1051/0004-6361/201731155.
- Matsumura, S., Brasser, R., Ida, S., 2021. N-body simulations of planet formation via pebble accretion. II. How various giant planets form. *Astronomy and Astrophysics* 650, A116. doi:10.1051/0004-6361/202039210.
- Morbidelli, A., Lunine, J.I., O'Brien, D.P., Raymond, S.N., Walsh, K.J., 2012. Building Terrestrial Planets. *Annual Review of Earth and Planetary Sciences* 40, 251–275. doi:10.1146/annurev-earth-042711-105319.
- Mumma, M., Weissman, P., Stern, S., Levy, E., Lunine, J., 1993. Protostars and planets iii. *Levy & JI Lunine*, Univ. Az. Press: Tucson 1177.
- Ormel, C.W., Klahr, H.H., 2010. The effect of gas drag on the growth of protoplanets. Analytical expressions for the accretion of small bodies in laminar disks. *Astronomy and Astrophysics* 520, A43. doi:10.1051/0004-6361/201014903.
- Ormel, C.W., Liu, B., 2018. Catching drifting pebbles. II. A stochastic equation of motion for pebbles. *Astronomy and Astrophysics* 615, A178. doi:10.1051/0004-6361/201732562.
- Paardekooper, S.J., Baruteau, C., Kley, W., 2011. A torque formula for non-isothermal Type I planetary migration - II. Effects of diffusion. *Monthly Notices of the Royal Astronomical Society* 410, 293–303. doi:10.1111/j.1365-2966.2010.17442.x.
- Pollack, J.B., Hubickyj, O., Bodenheimer, P., Lissauer, J.J., Podolak, M., Greenzweig, Y., 1996. Formation of the Giant Planets by Concurrent Accretion of Solids and Gas. *Icarus* 124, 62–85. doi:10.1006/icar.1996.0190.
- Rice, W., Lodato, G., Pringle, J., Armitage, P., Bonnell, I., 2006. Planetesimal formation via fragmentation in self-gravitating protoplanetary discs. *Monthly Notices of the Royal Astronomical Society: Letters* 372, L9–L13.
- Schoonenberg, D., Ormel, C.W., Krijt, S., 2018. A lagrangian model for dust evolution in protoplanetary disks: formation of wet and dry planetesimals at different stellar masses. *Astronomy and Astrophysics* 620.
- Seager, S., Kuchner, M., Hier-Majumder, C.A., Militzer, B., 2007. Mass-Radius Relationships for Solid Exoplanets. *The Astrophysical Journal* 669, 1279–1297. doi:10.1086/521346.
- Shakura, N.I., Sunyaev, R.A., 1973. Black holes in binary systems. Observational appearance. *Astronomy and Astrophysics* 24, 337–355.
- Tanaka, H., Takeuchi, T., Ward, W.R., 2002. Three-Dimensional Interaction between a Planet and an Isothermal Gaseous Disk. I. Corotation and Lindblad Torques and Planet Migration. *The Astrophysical Journal* 565, 1257–1274. doi:10.1086/324713.
- Testi, L., Natta, A., Shepherd, D.S., Wilner, D.J., 2003. Large grains in the disk of CQ Tau. *Astronomy and Astrophysics* 403, 323–328. doi:10.1051/0004-6361:20030362.
- Thommes, E.W., Bryden, G., Wu, Y., Rasio, F.A., 2008. From Mean Motion Resonances to Scattered Planets: Producing the Solar System, Eccentric Exoplanets, and Late Heavy Bombardments. *The Astrophysical Journal* 675, 1538–1548.
- Thommes, E.W., Duncan, M.J., Levison, H.F., 1999. The formation of Uranus and Neptune in the Jupiter-Saturn region of the Solar System. *Nature* 402, 635–638. doi:10.1038/45185.
- Wang, H., Weiss, B.P., Bai, X.N., Downey, B.G., Wang, J., Wang, J., Suavet, C., Fu, R.R., Zucolotto, M.E., 2017. Lifetime of the solar nebula constrained by meteorite paleomagnetism. *Science* 355, 623–627. doi:10.1126/science.aaf5043.
- Weidenschilling, S.J., 1977. Aerodynamics of solid bodies in the solar nebula. *Monthly Notices of the Royal Astronomical Society* 180, 57–70. doi:10.1093/mnras/180.2.57.
- Weidenschilling, S.J., 1980. Dust to planetesimals: Settling and coagulation in the solar nebula. *Icarus* 44, 172–189. doi:10.1016/0019-1035(80)90064-0.
- Weiss, L.M., Marcy, G.W., 2014. The Mass-Radius Relation for 65 Exoplanets Smaller than 4 Earth Radii. *The Astrophysical Journal* 783, L6. doi:10.1088/2041-8205/783/1/L6.
- Wilner, D.J., D'Alessio, P., Calvet, N., Claussen, M.J., Hartmann, L., 2005. Toward Planetesimals in the Disk around TW Hydrae: 3.5 Centimeter Dust Emission. *The Astrophysical Journal* 626, L109–L112. doi:10.1086/431757.
- Wölfer, E., Budde, G., Kleine, T., 2023. Age and genetic relationships among cb, ch and cr chondrites. *Geochimica et Cosmochimica Acta* 361, 288–301.
- Yang, C.C., Johansen, A., Carrera, D., 2017. Concentrating small particles in protoplanetary disks through the streaming instability. *Astronomy and Astrophysics* 606.